

# Electrolytic deposition of TiC nanoparticles/Ag composite films and their optical properties

Li Yuan<sup>1,2</sup> ✉, Chunyan Zeng<sup>1,2</sup>, Xuzheng Qian<sup>3</sup>, Chen Gao<sup>1,2</sup>, Yue Lu<sup>1,2</sup>, Fuyi Chen<sup>4</sup>

<sup>1</sup>School of Materials Science and Engineering, Sichuan University of Science & Engineering, Zigong 643000, People's Republic of China

<sup>2</sup>Material Corrosion and Protection Key Laboratory of Sichuan Province, Zigong 643000, People's Republic of China

<sup>3</sup>State Key Laboratory of Special Surface Protection Materials and Application Technology, Wuhan Research Institute of Materials Protection, Wuhan 430030, People's Republic of China

<sup>4</sup>State Key Laboratory of Solidification Processing, Northwestern Polytechnical University, Xian 710072, People's Republic of China

✉ E-mail: ylcx@mail.nwpu.edu.cn

Published in Micro & Nano Letters; Received on 27th June 2017; Revised on 26th October 2017; Accepted on 13th February 2018

TiC nanoparticles/Ag composite films were successfully prepared on an indium tin oxide (ITO) substrate through co-electrodeposition, using the Ag plating solutions with minor addition of TiC nanoparticles, followed by heat treatment in vacuum. The X-ray diffractometer, scanning electron microscope and UV-Vis spectrophotometer were used to characterise phase composition, morphologies and optical properties of as-fabricated films, respectively. Experimental results show that only TiC and Ag phases are identified for the TiC nanoparticles/Ag composite films and TiC nanoparticles are incorporated tightly and uniformly on the surface of the composite films, without obvious clustering. The results of optical property test reveal that the TiC nanoparticles/Ag composite films have similar optical properties as thick silver films perforated with nanohole arrays, which will pave the way towards numerous potential applications of Ag nanohole arrays.

**1. Introduction:** A lot of attention has been given to optically thick metal film perforated with subwavelength hole arrays [1] for its unique optical properties and potential applications [2, 3], since the discovery of the extraordinary optical transmission (EOT) [1]. It provides a way to use and control photons in a manner analogous to that of the control of electrons in solids.

As for its particular optical behaviours, the origin of EOT is not fully understood. On one hand, surface plasmon polarisation is thought to play an important role in the origin of EOT [4–6]. On the other hand, the role of localised plasmon resonances (LSPRs) cannot be neglected [7–11]. Experiments on the dependence of EOT with the hole shape revealed the existence of another type of transmission resonances, which arise from LSPRs, supported by hole arrays [12, 13] or isolated holes [14–16]. Therefore, more related researches should be conducted to deepen our understanding of the mechanisms underlying the unique optical behaviours.

With regard to its potential applications, optically thick metal film perforated with subwavelength hole arrays was found to have many potential applications in the field of plasmonic sensors, metamaterials, photonic devices and so on [17–21], but related research is still in its infancy due to technical obstacles. In order to fabricate subwavelength elements, nanoimprint lithography [22], e-beam lithography [23], focused-ion beam writing [24] or more advanced and expensive lithography techniques based on multi-photon polymerisation [25–27] are usually introduced. Based on this advanced nanofabrication technology, complicated nanostructures with curious optical behaviours [such as three-dimensional (3D) photonic metamaterials, 3D invisibility cloak at optical wavelengths etc.] have been fabricated [25–27]. However, these techniques are typically limited to sub-micron dimensions patterning and can be very time consuming for fabrication of nanostructure with an area of square centimetres or larger.

In this Letter, TiC nanoparticles/Ag composite films were successfully prepared on an indium tin oxide (ITO) substrate by co-electrodeposition, using the Ag plating solutions with minor addition of TiC nanoparticles, followed by heat treatment in vacuum at 500°C for 6 h. To facilitate co-electrodeposition of

TiC nanoparticles, the process strategy of physical dispersion (a magnetic stirring) combined with chemical dispersion (addition of cationic surfactant) was employed. The phase composition, morphologies and optical properties of the films were characterised by X-ray diffractometer, scanning electron microscope (SEM) and UV-Vis spectrophotometer, respectively. The results of optical property test revealed that the TiC nanoparticles/Ag composite films have similar optical properties as thick silver film perforated with nanohole arrays. Our TiC nanoparticles/Ag composite films examples represent an advance towards robust structures through a facile and large-scale manufacturing approach, which will pave the way to many potential applications of Ag films perforated with nanohole array.

## 2. Experimental methods

**2.1. Preparation of the substrates:** In this work, ITO plates (with a sheet resistance of  $15 \Omega \text{ cm}^{-1}$ ) with the cut size of  $25 \text{ mm} \times 15 \text{ mm} \times 2 \text{ mm}$  were used as the substrates. All side faces of the specimen were sealed with epoxy, leaving a working area of  $3 \text{ cm}^2$ . The step-by-step cleaning procedure employed prior to plating consists of cleaning the substrate with acetone, ultrasonic cleaning in ethanol for 5 min and rinsing with distilled water. Then the working face of the ITO substrate was activated in an acidic solution (0.1 mol/l HCL) for 60 s, washed in distilled water again and then immersed immediately in the plating bath.

**2.2. Plating bath and operating conditions:** Pure silver and TiC/Ag composite films were electrodeposited at room temperature. The basic composition of this bath electrolyte was 50 g/l of  $\text{AgNO}_3$ , 50 g/l of  $\text{K}_2\text{S}_2\text{O}_5$ , 250 g/l of  $\text{Na}_2\text{S}_2\text{O}_3$  and 30 g/l of  $\text{Na}_2\text{SO}_3$ . All chemicals were analytic grade reagents. The pH of the bath was maintained 6.5 by addition of sulphamic acid when required. In the case of TiC/Ag composite films electrodeposition, TiC powders with 400 nm mean diameter and high purity were employed. In order to vary the TiC content in the composites films, different concentrations of TiC powders were added in above solution (at concentration of 3 and 6 g/l, respectively).

About 2 ml/l linear alkylbenzene sulphonate was added in above solution as an anionic surfactant to prevent the agglomeration of particles. The TiC particles were maintained suspended in the electrolytic bath under a magnetic stirring at 600 rpm for 24 h before deposition. The stirring was maintained at 400 rpm during electrodeposition.

A direct electrodeposition technique was used to prepare the pure silver films and TiC/Ag composite films. A 600 ml beaker containing 500 ml of the solution was employed as electrolytic cell. A platinum sheet was used as anode, and ITO plate was used as cathode and vertically maintained at a distance of 5 cm from the anode. The determination of deposition voltage (the cathode electrode potential) was based on cyclic voltammograms (CVs) electrochemical measurements. Electrochemical measurements were performed through a CHI660C electrochemical system at room temperature on a three-electrode cell, where the ITO plate was used as working electrode, a platinum plate as counter electrode and a saturated calomel electrode (SCE) as a reference electrode. CVs were measured in the potential range of 0 V (SCE) to  $-1$  V (SCE) at a potential sweep rate of 5 mV/s. This potential range was cathodic relative to open-circuit potential of the ITO plate. After electrodeposition, as-plated films were subsequently heat treated in vacuum at 500°C for 6 h, followed by natural cooling down to room temperature.

**2.3. Characterisation of the prepared films:** To determine the phase composition of as-fabricated films, X-ray diffraction (XRD) patterns were obtained through an X-Per-PRO diffractometer with Cu K $\alpha$  radiation ( $\lambda = 1.5418$  Å) at a scanning rate of 0.02°/s in the range of 7°–90°. The work potential and current were 40 kV and 40 mA, respectively. The surface morphology and cross-sectional micrographs of as-prepared films were characterised by SEM (TESCAN VEGA 3SBU). The optical properties of as-fabricated films were studied at normal incidence using a UV–Vis spectrophotometer (PerkinElmer Lambda 35) equipped with a slit of 1 mm.

### 3. Results and discussion

**3.1. CV and electrodeposition:** CV technique is a very useful tool to analyse the main features of a deposition process. In this work, CV was used to monitor the redox behaviour of Ag<sup>+</sup> on an ITO electrode in the bath electrolyte without and with TiC nanoparticles. The scanning rate was 5 mV/s, the initial potential was 0 V, and the scanning direction was from 0 to  $-1$  V and to 0 V. As shown in Fig. 1, in the absence of TiC particles, a cathodic current peak is observed at about  $-0.6$  V (SCE), which is attributed to the nucleation of Ag film on the ITO electrode. In the presence of TiC nanoparticles (3 g/l), a cathodic current peak is observed at about  $-0.75$  V (SCE), which is associated with TiC/Ag co-deposition. It can be seen that the reductive current peak in TiC/Ag electrolyte is more negative than that in Ag electrolyte, indicating that, electrochemically, more energy is required for electrodeposition of TiC/Ag film than that of Ag film. Moreover, compared to the Ag CV, there is a lower cathodic current density at most of the individual potential on TiC/Ag voltammogram, indicating that the presence of TiC nanoparticles inhibits the cathodic reduction of metallic cations. The result is consistent with the above result about the shift of reductive current peak. As the concentration of TiC powders in TiC/Ag electrolyte increases, the reductive current peak becomes more negative slightly and the cathodic current density decrease lightly (not shown here).

As is known to all, electrode potential determines the electrodeposition process of nucleation and growth kinetics, and overpotential is the electrochemical driving force of nucleation in the constant potential mode [28], therefore the deposition potential should be reasonably established. In this work, during direct electrodeposition process, the cathode electrode potential was  $-0.6$  and  $-0.75$  V

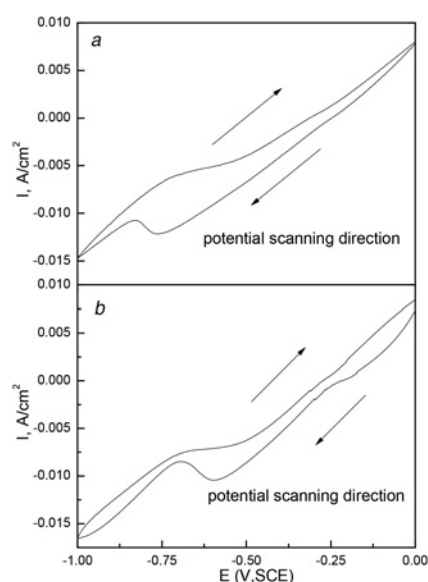


**Fig. 1** CVs measured on ITO electrode in the bath electrolyte with and without TiC nanoparticles  
a With TiC particles (3 g/l)  
b Without TiC particles

versus SCE for the electrodeposition of pure silver and TiC/Ag composite films, respectively. The plating time was set as 1 min. After electrodeposition, as-plated films were subsequently heat treated in vacuum at 500°C for 6 h.

**3.2. Characterisation of the prepared films:** The microstructure of as-prepared films was investigated by SEM. Fig. 2 shows the surface and cross-sectional morphologies of the pure silver film (film A) and TiC/Ag composite films electrodeposited from the plating bath containing 3 g/l (film B) and 6 g/l (film C) TiC nanoparticles. As illustrated in Fig. 2a, the surface morphology of the pure silver film is smooth and compact. Figs. 2b and c illustrate that the spherical TiC nanoparticles with a size  $\sim 10$ –550 nm (the histograms of TiC particle size distribution in individual composite films obtained by image analysis using Image-J software are present in Fig. 3, and the mean diameter of TiC particles is about 400 nm) are embedded tightly and evenly on the surface of the composite films without obvious agglomeration and the interfacial bonding between TiC nanoparticle and silver matrix is good. Compared to the TiC particle density in the film B, apparently, there are more TiC particles incorporated in the film C when the bath electrolyte contains a higher concentration of TiC nanoparticles, while a little TiC nanoparticle agglomeration is observed in the film C. According to Guglielmi's two-step adsorption model [29], the content of nanoparticles embedded into the film has some connection with adsorption of the particles during electrolytic deposition. When more particles are contained in the electrolyte, there will be a greater possibility to be adsorbed on the film for the particles. However, the agglomeration of particles becomes a problem when high concentrations of nanoparticles are added in the bath electrolyte. Therefore, in addition to the depositing method to reduce the particle agglomeration, such as the solution stirring and adding surfactants, there should be a balanced consideration of adsorption and agglomeration of nanoparticles on the film. Additionally, it is seen from Figs. 2d–f that the films and the substrates are combined compactly and no cracks or flaking off are observed at the interfaces between the films and the substrates. Besides that, it can be seen from Figs. 2d–f that all as-fabricated films have a thickness of about 1  $\mu$ m.

The phase composition of as-fabricated films was identified by XRD analysis. Fig. 4 shows the XRD pattern of the pure silver

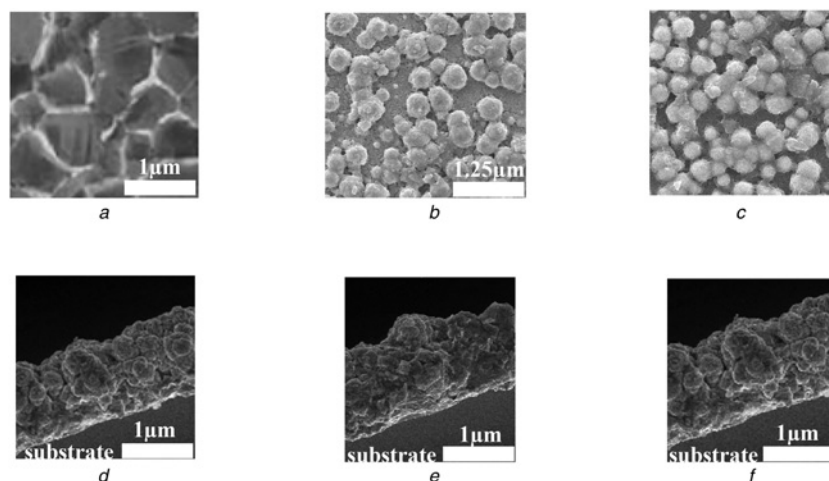


**Fig. 2** Surface morphologies of

*a* Pure Ag film

*b* TiC/Ag composite films electrodeposited from the plating bath containing 3 g/l nanoparticles

*c* Containing 6 g/l TiC nanoparticles

*d* Cross-sectional micrographs of pure Ag film

*e* TiC/Ag composite films electrodeposited from the plating bath containing 3 g/l nanoparticles

*f* Containing 6 g/l TiC nanoparticles

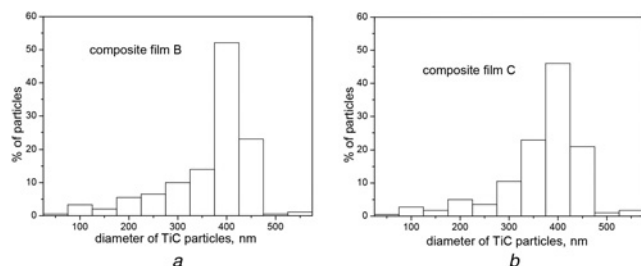


**Fig. 3** Histograms of TiC particle size distribution in TiC/Ag composite films electrodeposited from the plating bath containing

*a* 3 g/l (composite film B) TiC nanoparticles

*b* 6 g/l TiC nanoparticles (composite film C)

film and TiC/Ag composite films. As illustrated in Fig. 4*a*, only Ag diffraction peaks are identified for the pure silver film without adding TiC nanoparticles. The XRD patterns of TiC/Ag composite films electrodeposited from the plating bath containing 3 and 6 g/l TiC nanoparticles are shown in Figs. 4*b* and *c*, respectively. There are no obvious differences between the two XRD patterns. It is seen from Figs. 4*b* and *c* that except for strong Ag diffraction peaks, diffraction peaks around  $2\theta$  values of  $36^\circ$ ,  $42^\circ$  and  $61^\circ$  are detected, which correspond to the (1 1 1), (2 0 0) and (2 2 0) planes of a face-centered cubic phase of TiC, respectively. Additionally, compared to the XRD pattern of pure silver film, it can be found that the co-deposition of TiC particles with the silver deposit does not change the preferred orientation growth of silver crystals, while the related Ag diffraction peaks are weaker than those of the pure silver film, the more TiC nanoparticles the Ag plating solution contain, the weaker the related Ag diffraction peaks of corresponding TiC/Ag composite film become. The XRD analysis results are consistent with SEM analysis results. Hence, SEM and XRD analyses confirm the successful incorporation of TiC nanoparticles into the silver film.

**3.3. Optical properties of the prepared films:** The optical transmission coefficient spectrum of the pure silver film and TiC/Ag composite films in the wavelength range of 300–600 nm are illustrated in Fig. 5. As shown in Fig. 5*a*, the pure silver film (pure silver film A) with a thickness of about 1  $\mu\text{m}$  reveals a low

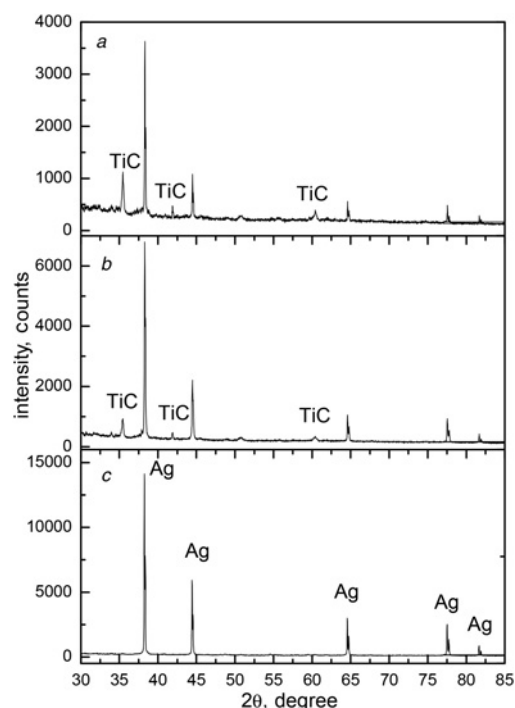


**Fig. 4** XRD patterns of

*a* Pure Ag film

*b* TiC/Ag composite films electrodeposited from the plating bath containing 3 g/l TiC nanoparticles

*c* Containing 6 g/l TiC nanoparticles

transmission coefficient lower than 5% in the wavelength range due to strong reflection and surface plasmon resonances absorption [9]. In comparison to the pure silver film without adding TiC nanoparticles, interesting light phenomena are observed for the TiC/Ag composite films electrodeposited from the plating bath containing 3 g/l (composite film B) and 6 g/l (composite film c) TiC nanoparticles. It can be seen from Figs. 5*b* and *c* that the TiC/Ag composite films have totally different optical behaviours from the pure silver film: two strong

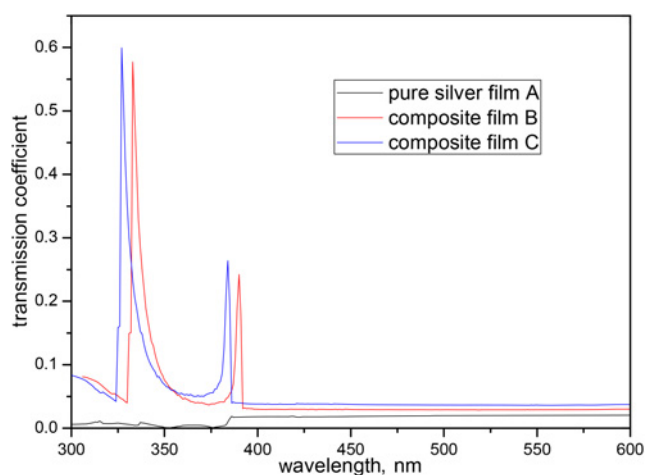


**Fig. 5** Transmission coefficient spectrum in the wavelength range of 300–600 nm for pure Ag film A and TiC/Ag composite films electrodeposited from the plating bath containing 3 g/l (composite film B) and 6 g/l (composite film C) TiC nanoparticles

transmission coefficient peaks are present in the optical transmission coefficient spectrum for the composite film B and composite film C, respectively. Additionally, the two transmission coefficient peaks are red shifted in the optical transmittance coefficient spectrum for composite film C, compared to those in the optical transmittance coefficient spectrum for composite film B, which arise from the increase of particle density of TiC in the composite film, as shown in Figs. 4b and c. The above observed optical behaviours for as-prepared TiC/Ag composite films are similar to those of thick silver film perforated with nanohole arrays.

In our previous work about the optical properties of thick silver film perforated with nanohole arrays [19–21, 30], two extraordinary transmission coefficient peaks are observed in the optical transmission coefficient spectrum of thick silver film perforated with nanohole arrays. Related numerical simulations reveal that the two transmission coefficient peaks can be attributed to the coupling between top and down surface plasmon polaritons of the silver film, mediated by localised surface plasmon resonances supported by the metallic nanoholes. Accordingly, two types of coupling modes are formed: the symmetry coupling mode and the antisymmetric coupling mode, which are corresponding to transmission coefficient peak at long wavelength and transmission coefficient peak at short wavelength, respectively. Moreover, the linewidth, the strength and the position of two extraordinary transmission coefficient peaks can be further tuned by changing the hole shape, period of hole arrays and thickness of the metal film for the metal nanohole arrays based on realistic needs. Here, in the case of TiC/Ag composite films, it is thought that TiC nanoparticles play the same role as nanoholes: the TiC nanoparticles on the surface of TiC/Ag composite films play the role as assisting the coupling between film's electromagnetic surface modes and incidence light. Consequently, two types of coupling modes are formed: the symmetry coupling mode and the antisymmetric coupling mode, which are corresponding to transmission coefficient peak at long wavelength and transmission coefficient peak at short wavelength, respectively. Furthermore, the position of two strong transmission coefficient peaks of TiC/Ag composite films can be tuned by changing the particle density of TiC in the composite film, as shown in Figs. 4b and c.

Based on the two extraordinary transmission coefficient peaks, thick silver nanohole arrays present potential applications in the field of plasmonic sensors, optical magnetic metamaterials, photonic devices and so on [17–21]. However, fabrication of metal nanohole arrays usually needs nanoimprint lithography, e-beam lithography, focused-ion beam writing or more advanced and

expensive lithography techniques, which are, however, limited to sub-micron dimensions patterning and can be very time consuming for fabrication of nanostructure with an area of square centimetres or larger. Compared to the time-consuming and expensive fabrication technology of metal nanohole arrays, the co-electrodeposition technology is highly efficient and facile, therefore as-prepared TiC/Ag composite films show a high potential for applications in plasmonic sensors, optical magnetic metamaterials, photonic devices and so on, based on the similar optical properties as thick silver nanohole arrays.

The optical properties of TiC/Ag composite films depend on the distribution of TiC nanoparticles incorporated in the composite film. However, various electrodeposition parameters, such as the TiC nanoparticle and surfactant concentration in the bath electrolyte, the stirring rate, deposition potential and temperature, affect remarkably the TiC nanoparticle deposition and thus the film optical performance. Therefore, a few more studies need to be done in more detail in order to realise the control of TiC nanoparticle distribution in the composite film and thus the control of optical properties of TiC/Ag composite films. A related investigation is currently underway.

**4. Conclusion:** In this Letter, TiC nanoparticles/Ag composite films were successfully fabricated on an ITO substrate through co-electrodeposition and followed by heat treated in vacuum at 500°C for 6 h. Experimental results show that: (i) the TiC nanoparticles are incorporated evenly and tightly on the surface of the composite films without obvious agglomeration, meanwhile the interfacial bonding between TiC nanoparticles and silver matrix is good; (ii) as-prepared films have a good adhesion to the substrates and no cracks or flaking off are observed at the interfaces between the films and the substrates; (iii) two transmission coefficient peaks are present in the optical transmission coefficient spectrum of TiC nanoparticles/Ag composite films, additionally, the position of two transmission coefficient peaks of TiC/Ag composite films can be tuned by changing the particle density of TiC in the composite film. It is thought that the two transmission coefficient peaks can be attributed to the coupling between top and down surface plasmon polaritons of the silver film, consequently, symmetry coupling mode and antisymmetric coupling mode form. The TiC nanoparticles on the surface of TiC/Ag composite films play the role as assisting the coupling between film's electromagnetic surface modes and incidence light, just like the nanohole arrays in the case of thick silver nanohole arrays. Accordingly, the position of two strong transmission coefficient peaks of TiC/Ag composite films can be tuned by changing the particle density of TiC in the composite film. Based on similar optical properties as thick silver nanohole arrays, as-prepared TiC/Ag composite films show a high potential for applications in plasmonic sensors, optical magnetic metamaterials, photonic devices and so on, due to high efficiency and facility of the co-electrodeposition technology, compared to the time-consuming and expensive fabrication technology of metal nanohole hole arrays.

The study is just a test to invest the optical properties of TiC/Ag composite films. There are still some works needed to be done in more detail, such as the mechanism of TiC nanoparticles incorporation, the control of TiC nanoparticle distribution in the composite films, the characteristics of surface plasmon resonances in TiC/Ag composite films, the effect of TiC particle size and film thickness on the optical properties of composite films and so on. Further investigation is currently underway.

**5. Acknowledgments:** This work was supported by the National Natural Science Foundation of China (grant nos. 51271148 and U1633118), the Research Fund of Material Corrosion and Protection Key Laboratory of Sichuan Province in China (grant



## 6 References

- [1] Ebbesen T.W., Lezec H.J., Ghaemi H.F., *ET AL.*: 'Extraordinary optical transmission through sub-wavelength hole arrays', *Nature*, 1998, **391**, pp. 667–669
- [2] Scorrano L., Tricarico S., Bilotti F.: 'Resonating plasmonic particles to achieve power transmission enhancement through subwavelength apertures', *IEEE Photonics Technol. Lett.*, 2010, **22**, (12), pp. 938–940
- [3] Nishijima Y., Adachi Y., Rosa L., *ET AL.*: 'Augmented sensitivity of an IR-absorption gas sensor employing a metal hole array', *Opt. Mater. Express*, 2013, **3**, (7), pp. 968–976
- [4] Coe J.V., Garcia-Vidal F.J., Teeterskennedy S., *ET AL.*: 'Extraordinary transmission of metal films with arrays of subwavelength holes', *Annu. Rev. Phys. Chem.*, 2008, **59**, (59), pp. 179–202
- [5] Wu J.J., Lin H.E., Yang T.J., *ET AL.*: 'Low-frequency surface plasmon polaritons guided on a corrugated metal striplines with subwavelength periodical inward slits', *Plasmonics*, 2011, **6**, (1), pp. 59–65
- [6] Xiang D., Wang L.L., Zhai X., *ET AL.*: 'Optical transmission through metal/dielectric multilayer films perforated with periodic subwavelength slits', *Opt. Commun.*, 2011, **284**, (1), pp. 471–475
- [7] Gao D., Chen W., Mulchandani A., *ET AL.*: 'Detection of tumor markers based on extinction spectra of visible light passing through gold nanoholes', *Appl. Phys. Lett.*, 2007, **90**, pp. 073901–073904
- [8] Chang S.H., Gray S., Schatz G.: 'Surface plasmon generation and light transmission by isolated nanoholes and arrays of nanoholes in thin metal films', *Opt. Express*, 2005, **13**, (8), pp. 3150–3165
- [9] Parsons J., Hendry E., Burrows C.P., *ET AL.*: 'Localized surface-plasmon resonances in periodic nondiffracting metallic nanoparticle and nanohole arrays', *Phys. Rev. B: Condens. Matter Mater. Phys.*, 2009, **79**, pp. 073412–073415
- [10] Zheng H., Vallée R., Rui M.A., *ET AL.*: 'Quasi-total omnidirectional light absorption in nanostructured gold films', *Appl. Phys. A*, 2014, **117**, (2), pp. 471–475
- [11] Christ A., Zentgraf T., Tikhodeev S.G., *ET AL.*: 'Controlling the interaction between localized and delocalized surface plasmon modes: experiment and numerical calculations', *Phys. Rev. B*, 2006, **74**, (15), pp. 2952–2961
- [12] Li J.Y., Hua Y.L., Fu J.X., *ET AL.*: 'Influence of hole geometry and lattice constant on extraordinary optical transmission through subwavelength hole arrays in metal films', *J. Appl. Phys.*, 2010, **107**, (7), pp. 667–671
- [13] Degiron A., Ebbesen T.W.: 'The role of localized surface plasmon modes in the enhanced transmission of periodic subwavelength apertures', *J. Opt. A, Pure Appl. Opt.*, 2005, **7**, pp. S90–S96
- [14] Fiala J., Richter I.: 'Interaction of light with subwavelength apertures: a comparison of approximate and rigorous approaches', *Opt. Quantum Electron.*, 2009, **41**, (5), pp. 409–427
- [15] Lee J.W., Seo M.A., Kang D.H., *ET AL.*: 'Terahertz electromagnetic wave transmission through random arrays of single rectangular holes and slits in thin metallic sheets', *Phys. Rev. Lett.*, 2007, **99**, (13), pp. 137401–137404
- [16] Wenger J., Dintinger J., Bonod N., *ET AL.*: 'Raman scattering and fluorescence emission in a single nanoaperture: optimizing the local intensity enhancement', *Opt. Commun.*, 2006, **267**, (1), pp. 224–228
- [17] Gustafsson M., Sjöberg D.: 'Sum rules and physical bounds on passive metamaterials', *New J. Phys.*, 2010, **12**, (4), pp. 043046–043063
- [18] Valentine J., Zhang S., Zentgraf T., *ET AL.*: 'Three-dimensional optical metamaterial with a negative refractive index', *Nature*, 2008, **455**, (7211), pp. 376–379
- [19] Chen F., Yuan L., Johnston L.: 'Low-loss optical magnetic metamaterials on Ag–Au bimetallic fishnets', *J. Magn. Magn. Mater.*, 2012, **324**, pp. 2625–2630
- [20] Yuan L., Chen F.: 'Optical magnetic metamaterials based on thick metal film perforated with rectangular nanohole arrays', *Phys. Status Solidi B*, 2013, **250**, pp. 1651–1654
- [21] Yuan L., Chen F.: 'Plasmonic sensors based on thick metal film perforated with rectangular nanohole arrays', *Physica Status Solidi RRL*, 2013, **7**, pp. 562–565
- [22] Wu W., Yu Z., Wang S., *ET AL.*: 'Midinfrared metamaterials fabricated by nanoimprint lithography', *Appl. Phys. Lett.*, 2007, **90**, pp. 063107–063110
- [23] Liu N., Guo H., Fu L., *ET AL.*: 'Three-dimensional photonic metamaterials at optical frequencies', *Nature Mater.*, 2008, **7**, pp. 31–37
- [24] Enkrich C., Pérez-Willard F., Gerthsen D., *ET AL.*: 'Focused-Ion-Beam nanofabrication of near-infrared magnetic metamaterials', *Adv. Mater.*, 2005, **17**, pp. 2547–2549
- [25] Rill M.S., Plet C., Thiel M., *ET AL.*: 'Photonic metamaterials by direct laser writing and silver chemical vapour deposition', *Nature Mater.*, 2008, **7**, pp. 543–546
- [26] Gansel J.K., Thiel M., Rill M.S., *ET AL.*: 'Gold helix photonic metamaterial as broadband circular polarizer', *Science*, 2009, **325**, pp. 1513–1515
- [27] Ergin T., Stenger N., Brenner P., *ET AL.*: 'Three-dimensional invisibility cloak at optical wavelengths', *Sci.*, 2010, **328**, pp. 337–339
- [28] Rezaei B., Damiri S.: 'Electrodeposited silver nanodendrites electrode with strongly enhanced electrocatalytic activity', *Talanta*, 2010, **83**, (1), pp. 197–204
- [29] Yao Y., Yao S., Zhang L., *ET AL.*: 'Electrodeposition and mechanical and corrosion resistance properties of Ni–W/SiC nanocomposite coatings', *Mater. Lett.*, 2007, **61**, pp. 67–70
- [30] Yuan L., Chen F.: 'Characteristics of surface plasmon resonances in thick metal film perforated with nanohole arrays', *Optik*, 2016, **127**, pp. 3504–3508
- [31] Burckel D.B., Wendt J.R., Ten Eyck G.A., *ET AL.*: 'Micrometer-scale cubic unit cell 3D metamaterial layers', *Adv. Mater.*, 2010, **22**, pp. 5053–5057